



Oxidation of organic pollutants by peroxymonosulfate activated with low-temperature-modified nanodiamonds: Understanding the reaction kinetics and mechanism



Eun-Tae Yun^{a,1}, Gun-Hee Moon^{b,1}, Hongshin Lee^c, Tae Hwa Jeon^b, Changha Lee^c, Wonyong Choi^b, Jaesang Lee^{a,*}

^a School of Civil, Environmental, and Architectural Engineering, Korea University, Seoul, 136-701, Republic of Korea

^b Division of Environmental Science and Engineering & Department of Chemical Engineering, Pohang University of Science and Technology (POSTECH), Pohang, 37673, Republic of Korea

^c School of Urban and Environmental Engineering, KIST-UNIST Ulsan Center for Convergent Materials (KUUC), Ulsan National Institute of Science and Technology (UNIST), 50 UNIST-gil, Ulsan, 44919, Republic of Korea

ARTICLE INFO

Keywords:

Nanodiamond
Low-temperature modification
Peroxymonosulfate activation
Non-radical mechanism
Electron transfer

ABSTRACT

Changes in surface carbon hybridization through high-temperature annealing ($> 1000^{\circ}\text{C}$) of nanodiamond (ND), i.e., surface graphitization, enable peroxymonosulfate (PMS) activation by ND. Alternatively, this study suggests low-temperature surface modification (500°C) of ND as an effective strategy for allowing ND to activate PMS. ND calcination in the presence of poly(diallyldimethylammonium chloride) (PDDA) and graphene oxide (GO) in an NH_3 atmosphere produced binary and ternary nitrogen-doped ND composites (i.e., N-ND/PDDA and N-ND/PDDA/GO). Compared with bare ND, these surface-modified NDs markedly enhanced organic oxidation associated with PMS activation. In particular, N-ND/PDDA/GO outperformed graphitized ND in terms of PMS activation capacity. Spectroscopic characterization implied that the content of pyridinic N and the N doping level increased with further modification of ND. Oxidation by PMS activated with ND-based materials did not involve radical attack, as methanol did not exhibit a quenching effect, formaldehyde yield was insignificant, conversion of bromide into bromate was negligible, the substrate specificity contradicted sulfate radical ($\text{SO}_4^{\cdot-}$) reactivity, and no electron paramagnetic resonance spectral features were assignable to $\text{SO}_4^{\cdot-}$ adducts. Impedance spectroscopic analysis indicated a high correlation between PMS activation efficacy and electrical conductivity. Chronoamperometric measurements showed that sequential injection of PMS and 4-chlorophenol caused current generation at electrodes coated with ND-based activators, and the increase in current intensity correlated well with PMS activation capacity. These findings suggest that ND-derived materials facilitated the electron transfer from organics to PMS, resulting in a degradative reaction route not reliant on radical species.

1. Introduction

Persulfate (collectively indicating peroxymonosulfate (PMS) and peroxydisulfate (PDS)) activation processes represent physicochemical strategies that initiate the production of sulfate radicals ($\text{SO}_4^{\cdot-}$) and the associated oxidative treatment of organics through the homolytic or heterolytic scission of peroxide bonds in persulfates [1,2]. The powerful oxidizing capacity of $\text{SO}_4^{\cdot-}$ ($E^{\circ}(\text{SO}_4^{\cdot-}/\text{SO}_4^{2-}) = 2.5\text{--}3.1 \text{ V}_{\text{NHE}}$ [3]), which enables oxidative degradation and mineralization of a broad spectrum of organics [4–7], has brought increased research focus to persulfate activation processes as alternatives to H_2O_2 -based advanced

oxidation processes (AOPs). The peroxide bond dissociation energies of these oxyanions (92 kJ mol⁻¹ for PDS; 213 kJ mol⁻¹ for H_2O_2 [2]) indicate that O–O bond cleavage associated with radical production occurs more readily in PDS than in H_2O_2 under light or heat irradiation [8,9]. Further, as the electron accepting capacities of PMS and PDS are superior to that of H_2O_2 , their peroxide bonds are more vulnerable to reductive cleavage by diverse activators, including transition and noble metals [1,4,5,10], inorganic anions (e.g., Cl^- and OH^-) [11], and quinones [12]. Notably, only a few reagents, such as iron- and copper-based species, are available for activation of H_2O_2 as a radical precursor. Further, whereas H_2O_2 is hardly activated with carbonaceous

* Corresponding author.

E-mail address: lee39@korea.ac.kr (J. Lee).

¹ These authors contributed equally to this work.

nanomaterials, their potential as metal-free persulfate activators has been recently explored. Such activators (e.g., carbon nanotubes (CNTs) and graphene) outperform metal-derived ones in activating persulfate in terms of treatment efficiency and persulfate consumption [13].

Owing to the unique mechanical, optical, and electronic properties, markedly increasing attention has been focused on nanodiamond (ND) since it was first discovered in 1990 through carbon detonation under oxygen-deficient conditions [14,15]. Two overarching strategies to improve the electric conductivity and (electro)catalytic performance of ND include annealing at high temperatures, which increases the sp^2 carbon content on the surface (i.e., surface graphitization) [16], and surface doping with nitrogen or boron [17,18]. Unlike pristine ND which does not activate PMS, improved catalytic activity for the oxidation of organic pollutants in the presence of PMS was observed after annealing ND in an inert gas atmosphere [19,20]. Electrochemical measurements corroborated that a thermally generated graphitic carbon layer on ND enhanced the electron transfer process involving PMS [19,20], which was assumed to be the main cause of PMS activation on annealed ND. However, the reaction pathway for oxidative decomposition of organics by graphitized ND in the presence of PMS likely varies depending on the fate of PMS during the electron transfer process. Annealed ND kinetically promotes one-electron reduction of PMS to SO_4^{2-} as a highly reactive intermediate (radical-induced mechanism) [19], but ND can also effectively mediate two-electron transfer from organics to PMS (non-radical mechanism) [20]. The sp^2 to sp^3 carbon ratio on ND surfaces is highly dependent on the annealing temperature [16], and ND calcination at temperatures exceeding 1000 °C, a highly energy-intensive process, is typically performed to maximize the catalytic activity of ND [19,20]. A ND core has a thicker graphitic carbon outer shell with increasing synthesis temperature, which likely switches degradative reaction pathway initiated during PMS activation by annealed ND from radical-dominated oxidation to oxidative decomposition without radical formation [21,22].

Heteroatom doping in a carbon framework, which destroys the electroneutrality of adjacent carbon atoms to form charge sites, redistributing the spin and charge density on carbon atoms, has been demonstrated to enhance the electrocatalytic activity of carbonaceous materials, such as CNTs and graphene, for the oxygen reduction reaction (ORR) [18]. The content and chemical form of doped nitrogen can be tuned by varying the annealing temperature under an NH_3 atmosphere. The pyridinic N content in nanocarbon materials gradually augments as temperature increases up to 550 °C, and the further temperature elevation induces the occurrence of graphitic N [23]. Pyridinic N and graphitic N significantly improve the ORR activity of N-doped carbon materials by facilitating oxygen adsorption and dissociation, as well as enhancing the electron-transfer process [24]. Thus, N-doping is a possible approach to enable PMS activation on ND.

Based on the previous finding that kinetic control of electron transfer is crucial in ND-induced PMS activation [19,20], in this study, we explored three ND modification strategies to improve electric conductivity or surface affinity toward PMS: N-doping of ND (N-ND), incorporation of N-ND into the cationic polymer, poly(diallyldimethylammonium chloride) (PDDA; used as a linker to electrostatically bridge GO with ND and a secondary source of nitrogen dopant) (N-ND/PDDA), and further surface modification with graphene oxide (GO) (N-ND/PDDA/GO). As thermal annealing at 300–500 °C in ammonia gas successfully achieves concomitant N-doping and reduction of GO sheets [25], the introduction of N as a dopant may occur during ND annealing at relatively low temperatures (500 °C). Note that surface graphitization of ND for PMS activation is performed at temperatures exceeding 1000 °C [19,20]. The applicability of the ND-derived materials for PMS activation was evaluated based on multi-activity assessment and catalytic performance. The structural and surface properties of the ND-based activators were investigated with diverse spectroscopic techniques and the electron-transfer process during PMS activation was characterized using chronoamperometry and impedance spectroscopy.

To elucidate the activation mechanism, we monitored the oxidation reaction kinetics in the presence of radical quenchers (i.e., methanol (MeOH) and dimethyl sulfoxide (DMSO)), the formation yields of formaldehyde, bromate(BrO_3^-), and hydroxybenzoic acid, and the electron paramagnetic resonance (EPR) spectra of radical adducts during PMS activation by the ND derivatives.

2. Materials and methods

2.1. Reagents

The chemicals that were used as-received in this study include: benzoic acid (Sigma-Aldrich), bisphenol A (Aldrich), carbamazepine (Sigma-Aldrich), 4-chlorophenol (4-CP; Aldrich), 4-nitrophenol (Aldrich), nitrobenzene (Sigma), phenol (Sigma-Aldrich), 2,4,6-trichlorophenol (Sigma), OXONE® monopersulfate compound (Sigma-Aldrich), potassium bromide (Sigma), potassium bromate (Sigma), DMSO (Sigma), formaldehyde (Sigma), methanol (Sigma-Aldrich), perchloric acid (Sigma-Aldrich), sodium hydroxide (Sigma-Aldrich), phosphoric acid (Aldrich), and acetonitrile (J.T. Baker). Ultrapure deionized water (18 MΩ cm) produced from a Millipore system was used for the preparation of all experimental solutions and suspensions.

2.2. Preparation and characterization of ND-based activators

For surface modification of ND (uDiamond Allegro solution, Carbodeon Co.) with PDDA (20 wt% in H_2O , Sigma-Aldrich), 0.45 g of ND powder (obtained after washing ND particles via centrifugation and drying at 80 °C) was dispersed in 500 mL of an aqueous solution containing 10 mL of PDDA solution. The aqueous binary mixture of ND and PDDA was subjected to sonication for 90 min followed by centrifugation with ultrapure water to remove excess PDDA. ND powder coated with PDDA was resuspended in 500 mL of 0.1 g/L aqueous GO solution (GO was prepared according to the modified Hummer method [26]). The suspension was exposed to ultrasound for 90 min and the resulting product was collected by centrifugation. All ND samples, including pristine ND, ND coated with PDDA, and ND surface-modified with PDDA and GO, were dried at 80 °C and calcined at 500 °C for 1 h under NH_3 gas flow (100 mL/min) to produce the corresponding N-doped ND materials (i.e., N-ND, N-ND/PDDA, and N-ND/PDDA/GO). As a reference ND-based activator, surface-graphitized ND was prepared via thermal treatment of ND at 1000 °C for 2 h under a flowing argon atmosphere. To estimate the contents of impurities in the N-doped ND-based activators, a thermogravimetric analysis (TGA) was performed using pristine ND, N-ND, N-ND/PDDA, and N-ND/PDDA/GO under air (all tested samples were heated from 30 °C to 900 °C at a rate of 5 °C/min). Drastic weight loss occurred in the temperature range of 450 °C to 600 °C and the complete combustion was achieved when temperature increased up to ca. 650 °C (Fig. S1). Based on the TGA curves, the impurities in ND-derived materials corresponding to the incombustible mass were present at trace levels.

To identify the crystalline and amorphous carbon phases in the ND-based activators, X-ray diffraction (XRD) patterns were obtained with an X-ray diffractometer (Rigaku SmartLab) using Cu-K α radiation. Raman spectra were recorded on a LabRam ARAMIS Raman spectrometer (Horiba Jobin-Yvon) using an argon ion laser (excitation at 514.5 nm) to track changes in defect density and amorphous carbon concentration. The contents and chemical forms of nitrogen in ND-derived materials were analyzed by X-ray photoelectron spectroscopy (XPS, Thermo Scientific K-Alpha) using a monochromatic Al-K α X-ray source (1486.6 eV). The surface functional groups of the activators were monitored by Fourier transform infrared spectroscopy (FT-IR, Thermo Scientific Nicolet iS50) performed in attenuated total reflectance (ATR) mode with a ZnSe crystal. The Brunauer–Emmett–Teller (BET) surface areas and pore volumes were determined from N_2 adsorption/desorption isotherms at –196 °C using a Micrometrics ASAP2020 sorption

analyzer. High-resolution transmission electron microscopy (HRTEM; JOEL JEM-2200FS) was used to analyze the morphological features of ND-derived materials. The zeta potentials of ND-based materials were determined as a function of pH using a zeta potential and particle size analyzer (ELS-Z-1000, Otsuka Electronics Co.).

2.3. Experimental procedures and analytical methods

All experiments were carried out in a magnetically stirred 50-mL cylindrical reactor under air-equilibrated conditions. A typical experimental suspension contained 0.1 g/L ND-based activator, 1 mM PMS, and 0.1 mM target substrate. The aqueous suspensions were buffered at pH 7.0 using 1 mM phosphate. No significant pH change was observed during PMS activation. Sample aliquots of 1 mL were withdrawn from the reactor at predetermined time intervals using a 1-mL syringe, filtered through a 0.45 µm PTFE filter (Millipore), and transferred to a 2-mL glass vial for further analyses. Methanol (0.2 M) was added to quench any radical species formed during the sample storage. All experiments were performed in duplicate. Oxidative degradation of the target substrates was monitored by a high-performance liquid chromatography (HPLC) using an Agilent 1260 Infinity instrument equipped with a UV/vis detector (277 nm for 4-CP) and a C-18 column (ZORBAX Eclipse XDB-C18). The HPLC eluent was a binary mixture consisting of 0.1% (v/v) aqueous phosphoric acid and acetonitrile (60/40 by volume). The concentrations of ionic species, such as chloride (Cl^-), bromide (Br^-), and BrO_3^- , were measured by an ion chromatography (IC) using a Dionex DX-120 system equipped with a Dionex IonPac AS-14 column and a conductivity detector. PMS was quantified based on the spectrophotometric determination of iodine ($\lambda = 352 \text{ nm}$) formed via the reaction of PMS and iodide. As an indirect indication of oxidizing radical production, formaldehyde formation was monitored using HPLC after derivatization with 2,4-dinitrophenylhydrazine (DNPH). EPR analysis was performed using 5,5-dimethyl-1-pyrroline N-oxide (DMPO) as a spin-trapping agent for $\text{SO}_4^{\cdot-}$. The EPR spectra were monitored in aqueous suspensions containing ND-based activator and PMS using a JEOL JES-TE 300 spectrometer under the following conditions: microwave power = 0.998 mW, microwave frequency = 9.415 GHz, center field = 335 mT, modulation width = 0.2 mT, modulation frequency = 100 kHz, sweep time = 30 s.

2.4. Electrochemical measurements

To investigate the electron-transfer mediating action of ND-based activators electrochemically, we prepared carbon paper electrodes coated with pristine ND, N-ND, N-ND/PDDA, and N-ND/PDDA/GO (i.e., ND/CP, N-ND/CP, N-ND/PDDA/CP, and N-ND/PDDA/GO/CP electrodes) according to the following procedures. ND-based material (120 mg) and 29 µL of Nafion perfluorinated resin solution (5 wt%, Sigma-Aldrich) were added to 50 mL of 2-propanol. After ultrasonication of the suspension for 60 min, 20 µL of the mixture was dropped onto a carbon paper electrode, and the resultant electrode was dried at 100 °C for 10 min. This treatment was repeated 20 times to load the desired amount of ND-based material on the electrode. To estimate the conductivity enhancement for modified ND-based materials relative to pristine ND, electrochemical impedance spectroscopy was carried out using a potentiostat (VersaSTAT 3–400) under the following condition: applied constant potential of +1.0 V (vs. Ag/AgCl), AC voltage of 50 mV, frequency range of 1000 Hz–0.01 Hz, electrolyte solution of 0.2 M sodium perchlorate. ND- or modified ND-loaded carbon paper, Ag/AgCl, and coiled Pt wire electrodes were used as working, standard reference, and counter electrodes, respectively. For anoxic conditions, the experimental solution was purged with argon for 15 min prior to the measurement and maintained unstirred with the headspace continuously purged with argon during the experiment. The impedance spectroscopy results were analysed using an equivalent circuit corresponding to the specific activity in the electrochemical cell. Linear

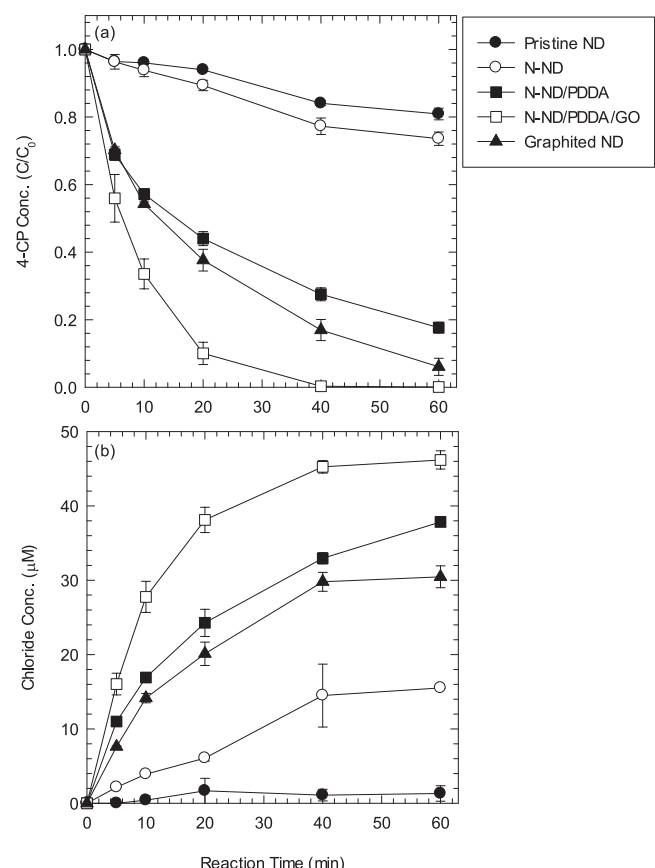


Fig. 1. (a) Oxidative degradation of 4-chlorophenol and (b) the associated evolution of chloride ions during PMS activation by nanodiamond-based activators ($[\text{activator}]_0 = 0.1 \text{ g/L}$; $[\text{PMS}]_0 = 1 \text{ mM}$; $[4\text{-chlorophenol}]_0 = 0.1 \text{ mM}$; $[\text{phosphate buffer}]_0 = 1 \text{ mM}$; $\text{pH}_i = 7.0$).

sweep voltammetry (LSV) and chronoamperometry experiments were conducted using a potentiostat (Ivium-n-Stat) with a three-electrode cell utilizing activator-loaded carbon paper, Ag/AgCl/KCl (sat), and pure carbon paper electrodes as the working, reference, and counter electrodes, respectively. For LSV, the current at the working electrode was recorded as the potential was swept from 0 to 1.4 V (vs Ag/AgCl) at a constant scan rate of 50 mV/s. Chronoamperometry was performed with the working electrode biased at an applied potential of +0.8 V (vs Ag/AgCl), allowing monitoring of current changes in response to the sequential addition of aliquots of oxyanion and 4-CP.

3. Results and discussion

3.1. PMS activation by ND-based materials

Fig. 1a shows a comparison of the PMS activation capacities of the ND-based materials (N-ND, N-ND/PDDA, and N-ND/PDDA/GO) based on the kinetic rate of oxidative degradation of 4-CP as a model substrate. Sorption on ND-based activators caused no noticeable reduction in 4-CP concentration (Fig. S2a). 4-CP was slightly degraded in the presence of PMS when applying pristine ND as an activator, which agrees with earlier findings on the inability of unmodified ND to activate PMS [19,20]. In contrast to the enhancing effect of N-doping on the PMS activation capacity of CNTs [27], only 27% of 4-CP was decomposed by PMS activated with N-ND over 60 min. In contrast, the incorporation of N-ND particles into the polymeric matrix (i.e., PDDA) markedly accelerated 4-CP degradation, which may be attributed to PDDA acting as a secondary nitrogen source to increase the N-doping level. A similar enhancement in PMS activation was achieved with

graphitized ND (Fig. 1a). However, it is noteworthy that N-ND/PDDA preparation required thermal treatment at 500 °C whereas surface graphitization required a calcination temperature of more than 1000 °C. The linkage of GO to N-ND/PDDA (achieved electrostatically with PDDA as a cationic binder) synergistically improved the PMS activation efficiency, with $k(4\text{-CP}) = 0.121 \text{ min}^{-1}$ for N-ND/PDDA/GO, $k(4\text{-CP}) = 0.035 \text{ min}^{-1}$ for N-ND/PDDA, and $k(4\text{-CP}) = 0.005 \text{ min}^{-1}$ for NH₃-treated PDDA/GO (without ND) (Fig. S2b). The 4-CP removal efficiency correlated well with the rate of chloride evolution owing to dechlorination (Figs. 1a and 1b), which confirmed that the oxidizing power of activated PMS was responsible for the decay of 4-CP. A gradual elevation in synthesis temperature caused the improvement in PMS activation efficiency of N-ND, N-ND/PDDA, and N-ND/PDDA/GO (Fig. S3), which was likely attributed to the transformation of sp³ to sp² carbon atoms. The observed enhancing effect became more pronounced with N-ND and N-ND/PDDA, but the composite resulting from further modification with GO exhibited excellent performance in PMS activation that remained almost constant irrespective of annealing temperature.

The comparative study using ND, ND/PDDA, and ND/PDDA/GO (prepared through thermal annealing at 500 °C in an argon atmosphere) also demonstrated that PDDA addition improved PMS activation capacity of the resultant composites (Fig. S4), which is likely compatible with highly promoted electrocatalytic activity of materials embedded in the PDDA polymer matrix. Binary and ternary composites synthesized without NH₃ treatment underperformed the corresponding composites, N-ND/PDDA and N-ND/PDDA/GO in oxidatively decomposing 4-CP in the presence of PMS. The superiority of N-ND/PDDA over ND/PDDA became more pronounced when comparatively evaluating the composites based on dechlorination efficiency (Fig. S4b), and thermal annealing in the presence of NH₃ led to a ten-fold increase in the kinetic rate of 4-CP oxidation by ND-based ternary composite (Fig. S4a). The result likely indicated more significant contribution of NH₃ to the N doping of ND-derived activators than PDDA. In particular, we observed that integration with GO drastically decreased the activity of ND/PDDA for 4-CP decay associated with PMS activation (Figs. S4a and b), which was in marked contrast to our finding on the enhancing effect of GO (Fig. 1a). This also revealed that only PDDA that served as a secondary N source could not achieve the effective N doping of nanocarbons (i.e., ND and GO). The low level N doping of GO was corroborated based on the comparison of the ATR-FTIR spectra of ND/PDDA and ND/PDDA/GO; a significant peak (centered 1200 cm⁻¹) assignable to the oxygen-containing chemical moieties (e.g., 1040 cm⁻¹ (C—O stretch) and 1164 cm⁻¹ (C—OH stretch) [28]) appeared in the spectrum of ND/PDDA/GO, whereas a broad peak corresponding to C—N bonds [29,30] formed in the spectrum of ND/PDDA (Fig. S5).

3.2. Activator properties related to PMS activation performance

HRTEM analysis of ND-based activators confirmed that calcination and surface modification resulted in negligible morphological changes (Fig. 2), with no formation of the onion-like carbon shells typically found in graphitized ND [19]. The TEM image of N-ND/PDDA/GO reveals that ND particles are dispersed on graphene sheets (Fig. S6). In order to clearly identify two distinct carbon nanostructures (i.e., ND and GO) on N-ND/PDDA/GO, fast Fourier transform (FFT) and inverse FFT were performed on two localized regions in the HRTEM image (Fig. S7). The green and red squares depicted ND and GO phases based on their morphological features. The FFT image and the corresponding inverse FFT image of the selected area (enclosed by the green square; Figs. S7b and c) showed diffraction pattern and lattice spacing typically found in the ND-based materials [31]. On the other hand, the images of the area marked by the red square (Figs. S7d and e) suggested the presence of the amorphous structure that likely resulted from N-doped GO [32].

The XRD patterns of all the ND-derived activators exhibited no

significant changes in peak intensity or full width at half maximum (FWHM) (Fig. 3a). The peaks located at 2θ = 43.8° and 75.3° correspond to diffractions from the (111) and (220) planes of cubic diamond, and the broad peak at 2θ = 21.9° indicates the presence of amorphous graphitic carbon [33,34]. These results collectively demonstrated that calcination in the presence of PDDA and GO at 500 °C under an NH₃ atmosphere did not achieve the diamond-to-graphite transition, implying that the enhanced activity of N-ND/PDDA and N-ND/PDDA/GO for PMS activation is not associated with a sp³ to sp² conversion of carbon atoms on ND surface (note that the sp² domain is responsible for effective persulfate activation on CNTs and graphitized NDs [19,20,35]). Analysis of the BET surface areas and pore volumes revealed that the pore volume of N-ND/PDDA/GO is slightly lower than those of the other ND-based materials, and the surface areas increase in the following order: N-ND < N-ND/PDDA < N-ND/PDDA/GO (Fig. S8d). The changes in surface area during activator preparation seem to correlate well with the PMS activating capacities of the ND-based activators. However, the difference in surface area between N-ND and N-ND/PDDA (or N-ND/PDDA/GO) (i.e., 257.49 and 267.42 cm²/g (or 291.80 cm²/g)) is not sufficient to account for several-fold increase in PMS activation efficiency via the incorporation of ND into PDDA (or further attachment of GO).

The Raman spectra of the ND-based activators (Fig. 3b) demonstrated no spectral changes after NH₃ treatment of pristine ND, but calcination in the presence of PDDA and GO caused ND to exhibit several broad peaks at 1328 cm⁻¹, 1410 cm⁻¹, 1459 cm⁻¹, 1590 cm⁻¹, and 1612 cm⁻¹, corresponding to diamond, D band, trans-polyacetylene, G-band, and O—H plus C=C bonds, respectively [14,36,37]. A comparison of the spectral features of N-ND/PDDA and N-ND showed that PDDA addition increases the intensity of the defect-sensitive D band, indicating a higher defect concentration in N-ND/PDDA [14]. The growth of the G band in the spectra of N-ND/PDDA and N-ND/PDDA/GO is likely attributable to an increase in the graphitic carbon concentrations owing to thermal annealing of PDDA and GO rather than ND. NH₃ treatment in the presence of PDDA produced a broad peak in the ATR-FTIR spectrum at 1060–1230 cm⁻¹, which is assigned to C—N bonds [29,30] (Fig. 3c). This characteristic peak became more intense in the spectrum of N-ND/PDDA/GO, which likely implies that more nitrogen is incorporated into the carbon lattices. The peak at around 1580 cm⁻¹ is indicative of the formation of aromatic ring structures [38]. Peaks corresponding to oxygen-containing chemical moieties were very weak [39], which suggests that oxygen groups may be reduced by NH₃.

Quantification of the surface elements using XPS revealed the presence of nitrogen on the surface of all the ND-based activators (elemental composition expressed in atomic percent (Fig. 3d) and weight percent (Fig. S9)), which is inevitable as nitrogen-containing precursors, such as trinitrotoluene and hexogen, are utilized for ND production [14]. No detectable amounts of metal impurities were found, except gold (reference material) and copper (substrate material) (Fig. S10). Although the oxygen content did not significantly vary with the type of modified ND-based activator, the surface nitrogen content (i.e., the N-doping concentration) gradually increased as ND was further modified (N-ND < N-ND/PDDA < N-ND/PDDA/GO) (Fig. 3d). The high-resolution N1s XPS spectra of the ND-based activators were deconvoluted to identify the chemical states of surface nitrogen (Figs. 4 a–d). The content of pyrrolic N, which was predominant in all tested activators, varied from 54% to 76%. A comparison of the N1s spectra of pristine ND and N-ND revealed that NH₃ treatment at 500 °C drastically reduced the content of oxidized N (from 21.1% to 12.5%) and removed nitrophenyl N (indicated by the peak at 406.0 eV) (Figs. 4a and b). In contrast, the peak at 398.2 eV, indicating the formation of pyridinic N, appeared after calcination of ND under an NH₃ atmosphere, with the peak intensity increasing in the following order: N-ND < N-ND/PDDA < N-ND/PDDA/GO. Although NH₃ treatment of ND decreased the content of graphitic N, recovery was observed following surface

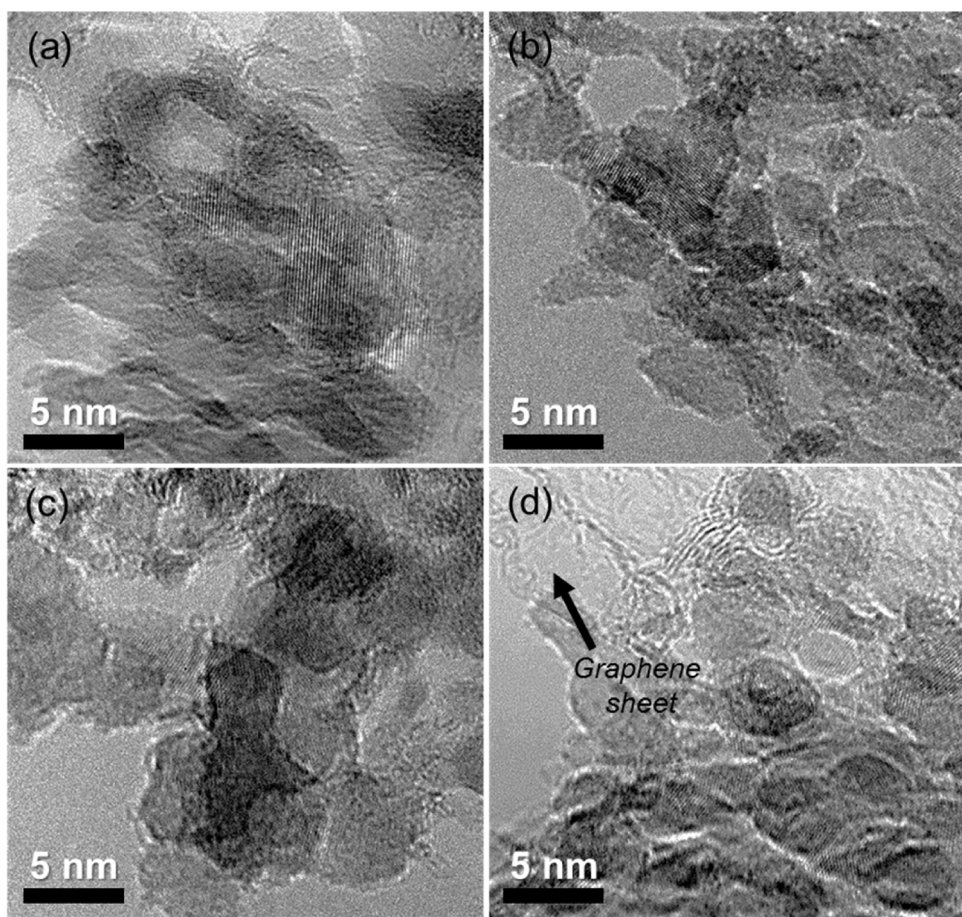


Fig. 2. High-resolution TEM images of (a) pristine ND, (b) N-ND, (c) N-ND/PDDA, and (d) N-ND/PDDA/GO.

modification of N-ND with PDDA and GO. Pyridinic N (causing a positive shift of on-set potential) and graphitic N (enlarging a limiting current density) have been demonstrated to enhance the electrocatalytic ORR by N-doped carbon materials [24], which supports the high performance of N-ND/PDDA and N-ND/PDDA/GO for PMS activation.

Embedding N-ND in the cationic polymer matrix shifted the zeta potential to a (more) positive value (Fig. S11). N-ND/PDDA exhibited a positive surface charge over a wide pH range, whereas bare ND was negatively charged and N-doping resulted in a neutral or negative charge in most cases. A positively charged activator will preferentially make direct contact with PMS, which primarily exists in its anionic form of HSO_5^- ($\text{pK}_{\text{a}1} = 0.4$; $\text{pK}_{\text{a}2} = 9.3$) [40,41]. Electrostatic attraction likely favors electron transfer to PMS (acting either as a radical precursor or as an electron acceptor), which could lead to the drastic enhancement in PMS activation and associated 4-CP degradation on N-ND/PDDA. Overall, the N-ND/PDDA and N-ND/PDDA/GO composites, characterized by effective N doping and high fractions of pyridinic N and graphitic N, are superior to pristine ND and N-ND in terms of conductivity and electron-transfer mediating capacity, which probably lead to the markedly improved PMS activation. In addition, the properties associated with higher PMS activation efficiencies likely include an increase in defect sites, a high surface area, and a PDDA-induced positive surface charge.

3.3. Oxidation pathway involving no radical attack

To explore the role of $\text{SO}_4^{\cdot-}$ as the main oxidant, we evaluated the PMS activation performance of the ND-based activators in the presence of methanol as a radical quencher (Fig. 5). No kinetic retardation of 4-

CP degradation was observed when applying excess methanol (molar ratio of methanol to 4-CP = 2000) (Fig. 5), which is consistent with the previous finding [20,35] that oxidizing radicals make a minor contribution to the oxidation of organics during persulfate activation on carbon-based nanomaterials (e.g., CNTs and graphitized ND). The formaldehyde formation yield also supported this finding, as no conversion of methanol to formaldehyde was observed with the ND-based activators, whereas formaldehyde production was significant with zero-valent iron nanoparticles (nFe° , which is known to produce $\text{SO}_4^{\cdot-}$ from PMS; prepared according to the method in [42]) (inset of Fig. 5). Considering that methanol may not scavenge radicals formed on hydrophobic carbon surfaces [43], 4-CP degradation by activated PMS was also examined in the presence of DMSO as an alternative quencher of $\text{SO}_4^{\cdot-}$ (Fig. S12). Similar to the results of Yao et al. [43], 4-CP degradation was apparently decelerated in the presence of DMSO. However, the significant reduction in 4-CP degradation efficiency was attributed not to the radical scavenging action of DMSO but to direct reduction of PMS by excess DMSO. PMS decomposition was gradually enhanced with increasing DMSO concentrations (inset of Fig. S12), which is consistent with the previous report on oxidative conversion of DMSO to dimethyl sulfone by PMS [44].

4-CP degradation by activated PMS was performed in the presence of alternative radical quenchers including ethanol, *tert*-butanol, and humic acid (HA) (note that ethanol and *tert*-butanol are effective for scavenging $\text{SO}_4^{\cdot-}$ and $\cdot\text{OH}$, respectively ($k_e(\text{ethanol} + \text{SO}_4^{\cdot-}) = 7.7 \times 10^7 \text{ M}^{-1}\text{s}^{-1}$; $k_b(\text{tert-butanol} + \cdot\text{OH}) = 7.6 \times 10^8 \text{ M}^{-1}\text{s}^{-1}$) [45]) (Fig. S13). Treatment performance reduction was virtually absent with ethanol and *tert*-butanol, which also revealed the minor role of oxidizing radicals in PMS activation by ND-based materials. The negligible kinetic inhibition in 4-CP oxidation may lead to the possibility that $\text{SO}_4^{\cdot-}$ strongly bound to hydrophobic

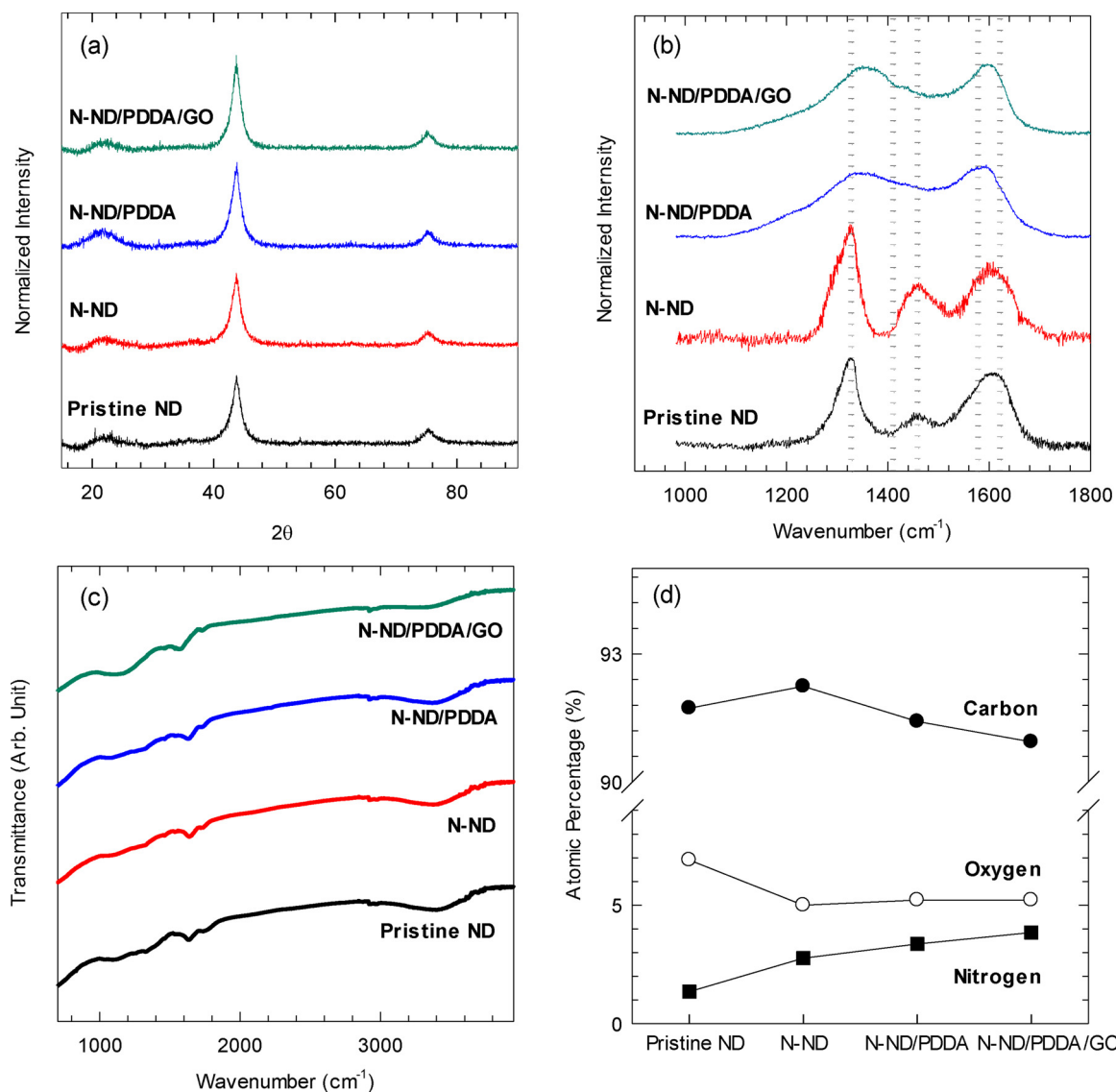


Fig. 3. (a) XRD patterns, (b) Raman spectra, (c) ATR-FTIR spectra, and (d) XPS surface elemental analyses of nanodiamond-based activators.

carbon surface could avoid quenching by highly water soluble alcohols, selectively reacting with 4-CP on the surface. Extremely low affinity of ND-based activators toward water likely hinders alcohols from eliminating surficial SO_4^{2-} , but at least it would allow partial quenching of surface-bound radical reactions in the presence of excess alcohols. It is noteworthy that ethanol effectively decelerated phenol oxidation during PMS activation by N-doped CNTs [46]. In contrast, 4-CP removal efficiency was drastically reduced upon addition of HA as a naturally occurring radical quencher [47] (Fig. S13). Considering that (i) overall radical scavenging activity of HA at the relatively low concentration ($\sim 200 \text{ mg/L}$) is not significant ($k_h[\text{HA}] = 6.8 \times 10^4 \text{ s}^{-1}$ versus $k_e[\text{ethanol}] = 1.54 \times 10^7 \text{ s}^{-1}$; Rate constant for HA oxidation by SO_4^{2-} (i.e., k_h) and carbon content of HA (on a molar basis) are estimated to be $6 \times 10^6 \text{ L} (\text{mol C})^{-1} \text{ s}^{-1}$ [47] and $232.3 \text{ mol C/mol HA}$ [48,49], respectively) and (ii) carbon-based nanomaterials exhibit high HA sorption capacity [50], the inhibitory effect of HA was attributable to surface coverage of N-ND/PDDA/GO with HA (HA outcompeted PMS for active surface sites on N-ND/PDDA/GO).

One-electron oxidation of halide ions by SO_4^{2-} leads to the formation of halogenated intermediates when oxidative degradation of organics by activated persulfate proceeds in the presence of excess halide ions [51,52]. As BrO_3^- is formed by the sequential oxidation of Br^- by SO_4^{2-} (i.e., $\text{Br}^- + \text{SO}_4^{2-} \rightarrow \text{HOBr}/\text{OBr}^- + \text{SO}_4^{2-} \rightarrow \text{BrO}_3^-$) [53], we monitored BrO_3^- production from Br^- when applying Co^{2+} and ND-based materials for PMS activation (Fig. 6a). Whereas Br^- was transformed stoichiometrically to BrO_3^- during PMS activation by Co^{2+} (leading to SO_4^{2-} formation), all the tested ND-based activators exhibited a negligible BrO_3^- formation yield. The EPR spectra of aqueous suspensions of N-ND, N-ND/PDDA, and N-ND/PDDA/GO showed direct oxidation of DMPO as a spin-trapping agent to 5,5-dimethylpyrrolidone-2-(oxy)-(1) (DMPOX) (Fig. 6b), which has markedly different spectral features than expected for the DMPO- SO_4^{2-} adduct [54]. DMPO could be converted to DMPOX through sequential reactions involving SO_4^{2-} [55]. However, considering that multifold results demonstrated so far pointed toward non-radical mechanism, the EPR detection of DMPOX is presumed to be another evidence that the dominant oxidative reaction pathway did not rely on SO_4^{2-} when activating PMS with ND-based materials.

Multi-activity assessment of eight organic compounds (benzoic acid, nitrobenzene, carbamazepine, 4-nitrophenol, phenol, bisphenol A, 4-CP, and trichlorophenol) confirmed that PMS activation activity decreases in the following order: N-ND/PDDA/GO > N-ND/PDDA > N-ND > pristine ND (Fig. 7). Regardless of the tested activator, the susceptibility to oxidation by activated PMS depended on the type of organic substrate, namely, oxidation of trichlorophenol was

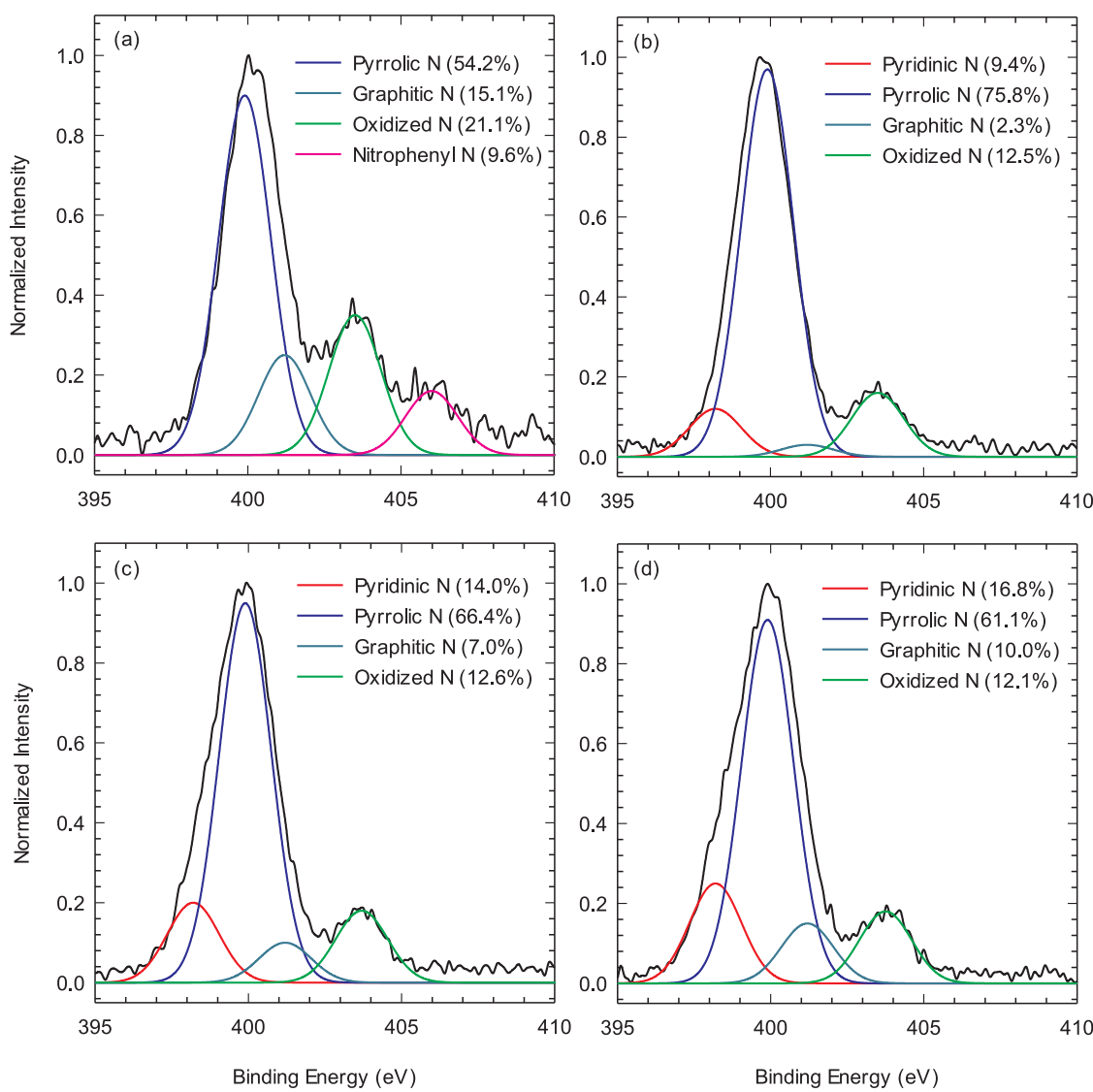


Fig. 4. High-resolution N1s XPS spectra of (a) pristine ND, (b) N-ND, (c) N-ND/PDDA, and (d) N-ND/PDDA/GO.

rapid; 4-CP, phenol, and bisphenol A were degraded at moderate rates; and 4-nitrophenol, nitrobenzene, carbamazepine, and benzoic acid were barely decomposed. This substrate-specific oxidation by activated PMS appeared to contradict the expected reactivity of $\text{SO}_4^{\cdot-}$. For example, carbamazepine degradation was almost absent (Fig. 7), but thermal and sonolytic activation of PDS (known to yield $\text{SO}_4^{\cdot-}$) is known to cause significant removal of carbamazepine [7,56]. Further, benzoic acid persisted during PMS activation by ND-based materials, but is highly vulnerable to $\text{SO}_4^{\cdot-}$ -induced oxidation ($k(\text{benzoic acid} + \text{SO}_4^{\cdot-}) = 1.2 \times 10^9 \text{ M}^{-1}\text{s}^{-1}$ [57]). Notably, no detectable amount of hydroxybenzoic acid was formed during benzoic acid oxidation by PMS activated with N-ND/PDDA/GO, whereas the alternative use of nFe° led to significant generation of the hydroxylated product as an indirect indication of $\text{SO}_4^{\cdot-}$ production (Fig. S14). Activation of peracetate (PA) as a precursor of hydroxyl radical ($\cdot\text{OH}$) with N-ND/PDDA/GO was not accompanied by the hydroxylation reaction. In contrast, a noticeable yield of hydroxybenzoic acid was obtained when nFe° was employed as the activator instead (Fig. S14).

Based on the previous report on successful PDS activation by N-doped GO (N-GO) [58], N-GO and N-GO/PDDA were prepared through thermal annealing of GO at 500 °C under an NH₃ atmosphere in the absence and presence of PDDA and were examined for PMS activation. In contrast to ND-based activators, PMS activation capacity of GO was

significantly decreased through incorporation into PDDA; N-GO outperformed N-GO/PDDA in degrading selected organics including carbamazepine, phenol, bisphenol A, 4-CP, and trichlorophenol (Fig. S15). The reduced PMS activation capacity of N-GO/PDDA is likely ascribed to the agglomeration of GO sheets in the presence of cationic PDDA polymers, which should be effectively hindered in N-ND/PDDA/GO because negatively charged ND particles can partially neutralize the positive charges derived from PDDA. Comparison of N-GO with N-ND/PDDA (or N-ND/PDDA/GO) (Fig. S15 versus Fig. 7) indicated that PMS activation was much more effectively performed when selecting ND composites, with $k(\text{trichlorophenol}) = 0.0052 \pm 0.0021 \text{ min}^{-1}$ for N-GO, $k(\text{trichlorophenol}) = 0.2034 \pm 0.0166 \text{ min}^{-1}$ for N-ND/PDDA, and $k(\text{trichlorophenol}) = 0.2522 \pm 0.0173 \text{ min}^{-1}$ for N-ND/PDDA/GO. Whereas the quenching effect of methanol was negligible on 4-CP degradation by ND-based activators (Fig. 5), 4-CP oxidation by N-GO and N-GO/PDDA was kinetically inhibited upon addition of methanol (Fig. S16), which appeared to match the earlier finding [59] that persulfate activation by GO and its derivatives was accompanied by $\text{SO}_4^{\cdot-}$ yield. The result contradicts the claim that methanol could not scavenge surficial $\text{SO}_4^{\cdot-}$ generated on hydrophobic carbon activators [43] (accordingly, no quenching effect of methanol presented in Fig. 5 is likely the evidence for non-radical oxidation pathway rather than for involvement of surface-bound $\text{SO}_4^{\cdot-}$). This also allows us to raise the

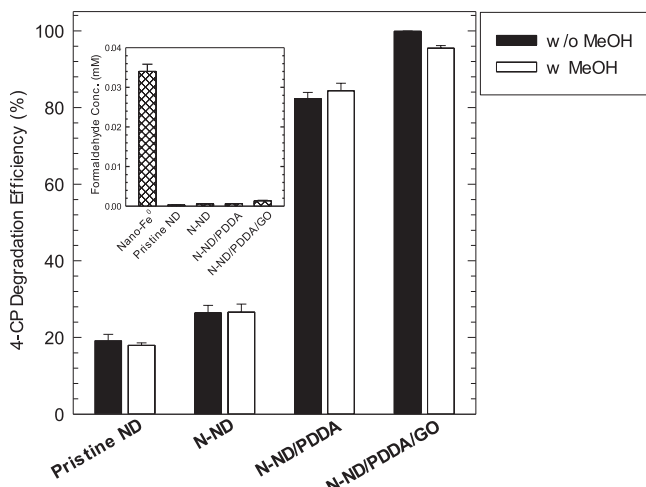


Fig. 5. Effect of methanol as a radical quencher on the 4-CP oxidation efficiencies of nanodiamond-based activators ([activator]₀ = 0.1 g/L; [PMS]₀ = 1 mM; [4-chlorophenol]₀ = 0.1 mM; [methanol]₀ = 200 mM; [phosphate buffer]₀ = 1 mM; pH_i = 7.0). Inset: Formaldehyde formation yields of zero-valent iron nanoparticles and nanodiamond-based materials ([nFe⁰]₀ = 0.05 g/L; [ND-based activator]₀ = 0.1 g/L; [PMS]₀ = 1 mM; [methanol]₀ = 10 mM; [phosphate buffer]₀ = 1 mM; pH_i = 7.0).

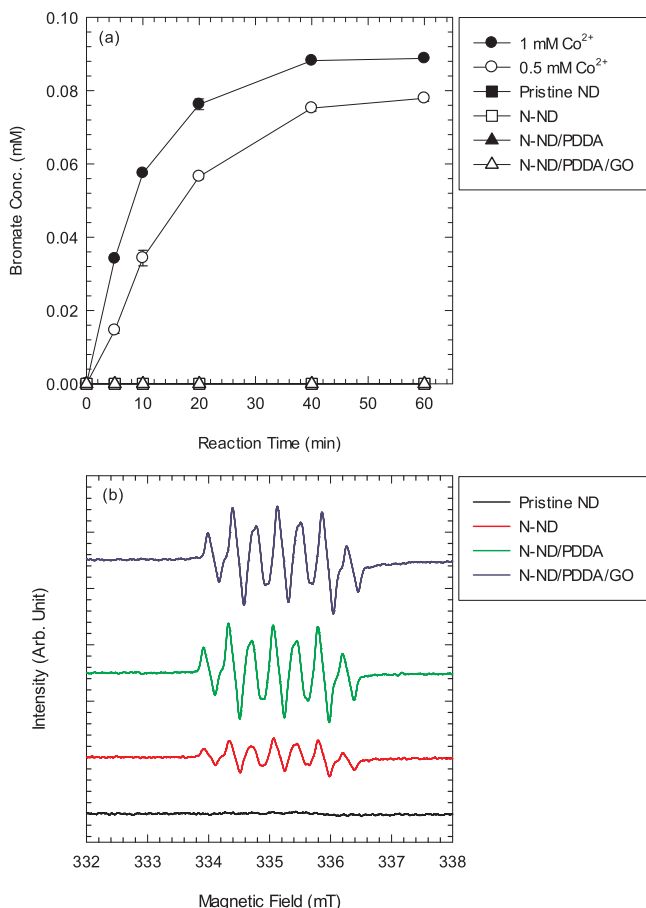


Fig. 6. (a) Formation of bromate during the oxidation of bromide ions by Co²⁺ and nanodiamond-based activators ([nanodiamond-based activator]₀ = 0.1 g/L; [PMS]₀ = 1 mM; [bromide]₀ = 0.1 mM; [phosphate buffer]₀ = 1 mM; pH_i = 7.0) and (b) EPR spectra of aqueous suspensions containing nanodiamond-based activators, PMS, and DMPO (spin-trapping agent) after 10 min of PMS activation ([activator]₀ = 0.1 g/L; [PMS]₀ = 1 mM; [DMPO]₀ = 1 mM; [phosphate buffer]₀ = 1 mM; pH_i = 7.0).

possibility that degradative reaction pathway initiated via persulfate activation may vary depending on the type of carbonaceous material.

3.4. Electron-transfer mechanism

The main factors controlling the persulfate activation capacity of carbonaceous nanomaterials include conductivity and surface properties (e.g., surface functionality and surface charge), which affect the kinetics of the electron-transfer process, as a key step in persulfate activation. Note that electron transfer to persulfate directly from the activator leads to SO₄²⁻ formation (radical mechanism), whereas indirect transfer from organic substrate via the activator causes pollutant oxidation (non-radical mechanism). Impedance spectroscopic analysis demonstrated that the sequential modification of ND with PDDA and GO remarkably reduced the charge transfer resistance (R_{ct}) at the ND-based activator/electrolyte interface in the presence of 4-CP and PMS (Fig. 8a). The R_{ct} values of ND, N-ND, N-ND/PDDA, and N-ND/PDDA/GO were determined to be 5.1, 4.1, 3.8, and 3.4 kΩ, respectively, by fitting the Nyquist plots to equivalent circuit diagram (Fig. 8a, inset). R_{ct} gradually decreased as calcination and surface modification proceeded, indicating that the PMS activation performance of ND-derived materials improves with increasing conductivity and electron-transfer mediating activity.

Fig. 8b demonstrates the chronoamperometry of carbon paper electrodes coated with ND-based activators (i.e., ND/CP, N-ND/CP, N-ND/PDDA/CP, and N-ND/PDDA/GO/CP electrodes) at an applied potential of + 0.8 V (vs Ag/AgCl) when PMS and 4-CP are added sequentially. No noticeable current changes at the pristine ND-deposited electrode were caused by the injection of PMS or 4-CP. The current intensity did not increase in response to PMS addition for any of the ND-based activator-loaded electrodes. In contrast, the subsequent addition of 4-CP resulted in significant current generation at the N-ND/PDDA/CP and N-ND/PDDA/GO/CP electrodes, which suggested that electron transfer is achievable in the co-presence of an electron donor (i.e., 4-CP), electron acceptor (PMS), and electron-transfer mediator (i.e., ND-derived material). ND-based activators can serve as electron-transfer mediators to facilitate electron delivery from organics to PMS, leading to oxidative degradation without radical attack [20,35,42]. In particular, the magnitude of the current jump correlated well with the PMS activation capacities of the ND-based materials (Figs. 1 and 8b). Both the current generation efficiency and PMS activation kinetics increased with further modification of ND through thermal annealing and integration with PDDA and GO (N-ND < N-ND/PDDA < N-ND/PDDA/GO). The superior performance of N-ND/PDDA/GO relative to the other activators in terms of current generation was also confirmed by LSV analysis (Fig. S17).

3.5. Catalytic performance

To explore the catalytic performance of the ND-based materials as PMS activators, repeated oxidative degradation of 4-CP through PMS activation was examined (Fig. 9). For each batch, the catalytic activity was evaluated by adding fresh 4-CP in each cycle. PMS was not externally supplied after the initial injection. The observed 4-CP degradation efficiencies over multiple cycles confirmed the superior performance of N-ND/PDDA/GO over the other ND-based activators. Irrespective of activator type, repeated use of the ND-derived materials led to a gradual loss of PMS activation capacity. As oxidation reaction route involving no radical attack likely allows carbonaceous nanomaterials to remain intact during repeated PMS activation, the reduction in PMS activation capacity may result from coverage of the active surface sites with intermediates and products generated during the oxidation of organics. The PMS activation activity was recovered by UV-C irradiation for 180 min (applied after the third catalytic cycle). This treatment could partially oxidize intermediates/products accumulated on the activator, regenerating the ND-based material. UV-C

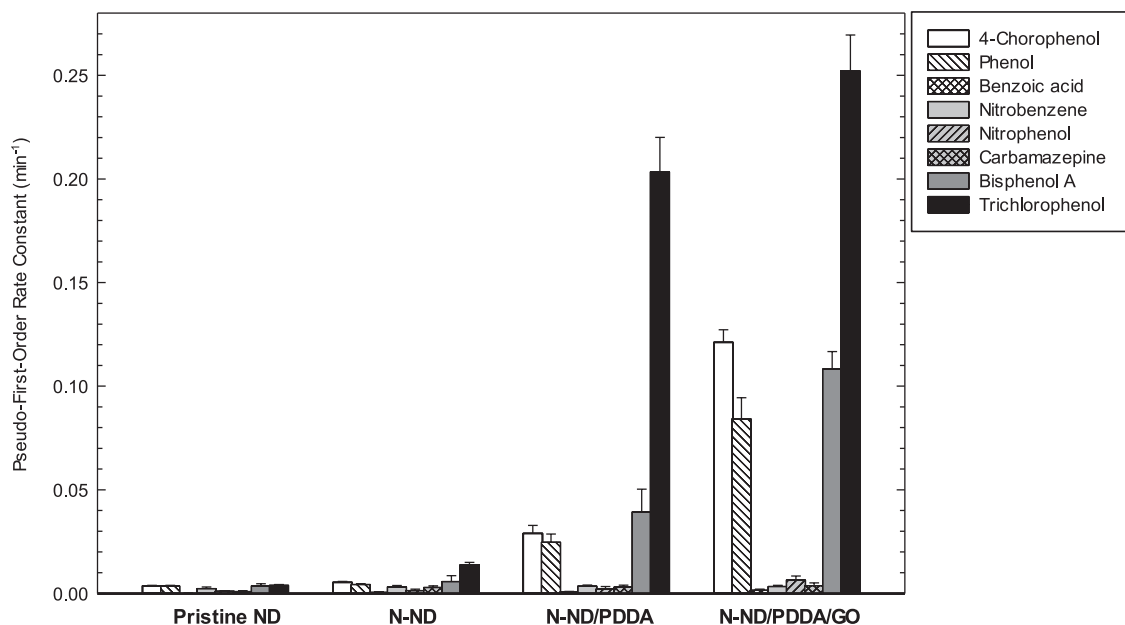


Fig. 7. Application of nanodiamond-based activators for the oxidative degradation of various organic substrates in the presence of PMS ($[activator]_0 = 0.1 \text{ g/L}$; $[\text{PMS}]_0 = 1 \text{ mM}$; $[\text{organic substrate}]_0 = 0.1 \text{ mM}$; $[\text{phosphate buffer}]_0 = 1 \text{ mM}$; $\text{pH}_i = 7.0$).

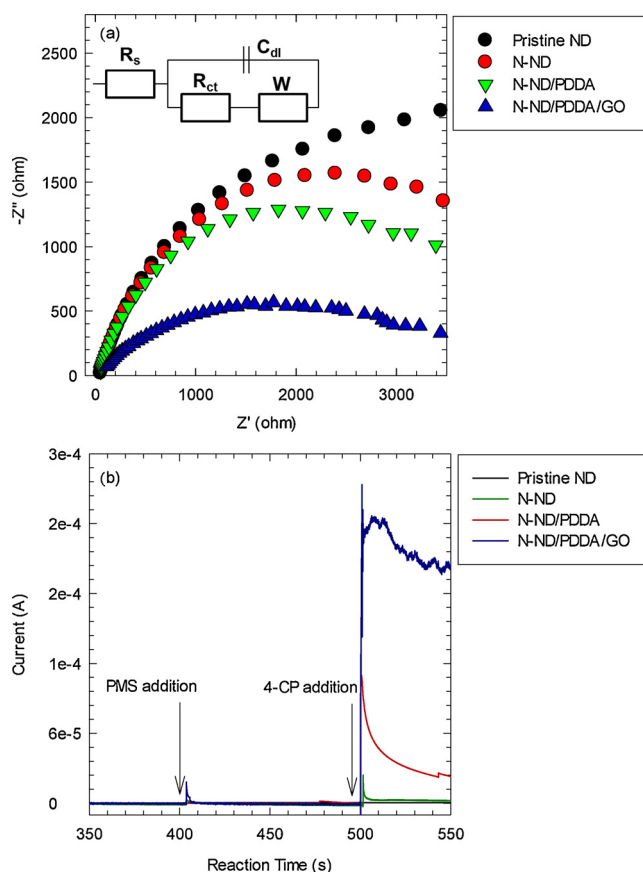


Fig. 8. (a) Electrochemical impedance spectroscopic analysis of carbon paper electrodes coated with nanodiamond-based activators ($[\text{NaClO}_4]_0 = 200 \text{ mM}$; $[\text{phosphate buffer}]_0 = 1 \text{ mM}$; $\text{pH}_i = 7.0$). Inset: Equivalent circuit diagram (C_{dl} , R_s , R_{ct} , and W indicate double layer capacitance, solution resistance, charge transfer resistance, and Warburg impedance, respectively). (b) Current generation at the electrode coated with nanodiamond-based activators upon PMS addition followed by 4-chlorophenol addition ($[\text{PMS}]_0 = 1 \text{ mM}$; $[\text{4-chlorophenol}]_0 = 0.1 \text{ mM}$; $[\text{phosphate bufer}]_0 = 1 \text{ mM}$; $\text{pH}_i = 7.0$).

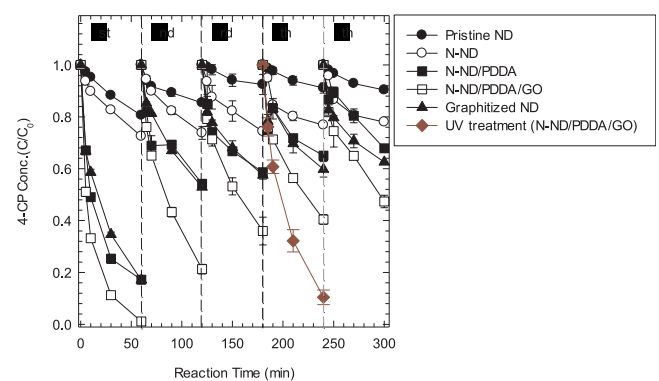


Fig. 9. Repeated application of nanodiamond-based activators for oxidative degradation of 4-chlorophenol in the presence of PMS ($[activator]_0 = 0.1 \text{ g/L}$; $[\text{PMS}]_0 = 1 \text{ mM}$; $[\text{4-chlorophenol}]_0 = 0.1 \text{ mM}$; $[\text{phosphate buffer}]_0 = 1 \text{ mM}$; $\text{pH}_i = 7.0$). Data is also shown for N-ND/PDDA/GO regenerated by UV-C treatment after the third catalytic cycle.

irradiation caused rapid 4-CP decay in the absence and presence of PMS (Fig. S18a), which ensured that direct UV-C photolysis or photochemical activation of residual PMS could decompose organics that may remain on carbon surface. On the other hand, formaldehyde oxidation was achieved only with photochemically activated PMS (Fig. S18b) since radical-induced pathway outperforms photo-transformation in degrading and mineralizing a wide range of organics. The presence of N-ND/PDDA/GO that likely serves as an inner filter and hinders light transmission through the aqueous suspensions led to the negligible kinetic retardation in photo-induced oxidation of organics. N-ND/PDDA/GO that was subjected to UV-C photolysis or photochemically generated oxidizing radicals (i.e., $\text{SO}_4^{\cdot-}$ and $\cdot\text{OH}$) was characterized by ATR-FTIR and Raman spectroscopy (Figs. S19a and b). Alteration in the IR spectral features was not pronounced and the intensity ratio of D-band to G-band (I_D/I_G) (reflecting the defect density of carbon-based materials) negligibly changed after UV-C irradiation in the absence and presence of PMS. The results ruled out the possibility that UV-based regeneration processes could significantly modify the surface chemical composition and defect density of ND-based activators.

4. Conclusion

In this study, we demonstrated that conductivity improvement (together with increases in surface area and defect sites, as well as a positively charged surface), achieved through incorporation into the cationic polymer matrix and integration with GO during thermal annealing under an NH₃ atmosphere, remarkably improved the PMS activation capacity of ND. Notably, the proposed ND modification technique was performed at 500 °C and did not involve surface graphitization, which typically occurs at temperatures exceeding 1000 °C. The substrate-specificity observed in the multi-activity assessment of multiple organics revealed that oxidative degradation initiated by ND-based activators is likely not ascribable to the oxidizing power of SO₄^{·-}. For instance, benzoic acid and carbamazepine, which are effectively degraded by SO₄^{·-}, underwent very slow decomposition during PMS activation on ND-based materials. A reaction pathway not reliant on radical species was further confirmed by empirical evidence. 4-CP oxidation was not retarded significantly in the presence of excess methanol as a radical quencher. Unlike nanoscale iron particles, which are able to produce SO₄^{·-} from PMS, none of the tested ND-based materials oxidized methanol into formaldehyde. BrO₃⁻ formation from Br⁻ was negligible when ND-based materials were used as PMS activators, in marked contrast to the effective oxidation of Br⁻ to the corresponding oxyanion by PMS activated with Co²⁺. Furthermore, PMS activated with ND-based materials did not exhibit the EPR spectral characteristics of the DMPO-SO₄^{·-} adduct. The PMS activation capacities of the ND-derived materials improved with decreasing charge transfer resistance (i.e., with increasing conductivity). A noticeable current increase at electrodes coated with the ND-based materials only occurred when sequentially injecting PMS and 4-CP. This observation suggested that electron transfer from organics (as an electron donor) to PMS (as an electron acceptor) facilitated by carbon-based nanomaterials (as an electron-transfer mediator) is likely responsible for the oxidizing capacity of PMS in the presence of ND-based activators.

Acknowledgments

This study was supported by the Basic Science Research Program (NRF-2017R1A2B4002235) and a grant from the National Research Foundation of Korea, funded by the Ministry of Science, ICT, and Future Planning (No. 2016M3A7B4909318);

Appendix A. Supplementary data

Supplementary material related to this article can be found, in the online version, at doi:<https://doi.org/10.1016/j.apcatb.2018.04.067>.

References

- [1] W.D. Oh, Z.L. Dong, T.T. Lim, *Appl. Catal. B: Environ.* 194 (2016) 169–201.
- [2] S. Waclawek, H.V. Lutze, K. Grübel, V.V.T. Padil, M. Černík, D.D. Dionysiou, *Chem. Eng. J.* 330 (2017) 44–62.
- [3] P. Neta, R.E. Huie, A.B. Ross, *J. Phys. Chem. Ref. Data* 17 (1988) 1027–1284.
- [4] G.P. Anipsitakis, D.D. Dionysiou, *Environ. Sci. Technol.* 37 (2003) 4790–4797.
- [5] J.K. Du, J.G. Bao, Y. Liu, H.B. Ling, H. Zheng, S.H. Kim, D.D. Dionysiou, *J. Hazard. Mater.* 320 (2016) 150–159.
- [6] Y.C. Lee, S.L. Lo, P.T. Chiueh, Y.H. Liou, M.L. Chen, *Wat. Res.* 44 (2010) 886–892.
- [7] J.M. Monteagudo, A. Duran, R. Gonzalez, A.J. Exposito, *Appl. Catal. B: Environ.* 176 (2015) 120–129.
- [8] C.J. Liang, C.F. Huang, Y.J. Chen, *Wat. Res.* 42 (2008) 4091–4100.
- [9] J. Saini, Z. Ojaghloo, A.R. Soleymani, M.H. Rasoulifard, *Chem. Eng. J.* 167 (2011) 172–182.
- [10] Y.Y. Ahn, E.T. Yun, J.W. Seo, C. Lee, S.H. Kim, J.H. Kim, J. Lee, *Environ. Sci. Technol.* 50 (2016) 10187–10197.
- [11] S.Y. Yang, P. Wang, X. Yang, L. Shan, W.Y. Zhang, X.T. Shao, R. Niu, *J. Hazard. Mater.* 179 (2010) 552–558.
- [12] G.D. Fang, J. Gao, D.D. Dionysiou, C. Liu, D.M. Zhou, *Environ. Sci. Technol.* 47 (2013) 4605–4611.
- [13] X.G. Duan, H.Q. Sun, J. Kang, Y.X. Wang, S. Indrawirawan, S.B. Wang, *ACS Catal.* 5 (2015) 4629–4636.
- [14] V.N. Mochalin, O. Shenderova, D. Ho, Y. Gogotsi, *Nat. Nanotechnol.* 7 (2012) 11–23.
- [15] N. Nunn, M. Torelli, G. McGuire, O. Shenderova, *Curr. Opin. Solid State Mater. Sci.* 21 (2017) 1–9.
- [16] M. Zeiger, N. Jackel, V.N. Mochalin, V. Presser, *J. Mater. Chem. A* 4 (2016) 3172–3196.
- [17] Y.M. Lin, D.S. Su, *Acs Nano* 8 (2014) 7823–7833.
- [18] X. Liu, L.M. Dai, *Nat. Rev. Mater.* 1 (2016) 16064.
- [19] X.G. Duan, C. Su, L. Zhou, H.Q. Sun, A. Suvorova, T. Odedairo, Z.H. Zhu, Z.P. Shao, S.B. Wang, *Appl. Catal. B: Environ.* 194 (2016) 7–15.
- [20] H. Lee, H.I. Kim, S. Weon, W. Choi, Y.S. Hwang, J. Seo, C. Lee, J.H. Kim, *Environ. Sci. Technol.* 50 (2016) 10134–10142.
- [21] X.G. Duan, Z.M. Ao, H.Y. Zhang, M. Saunders, H.Q. Sun, Z.P. Shao, S.B. Wang, *Appl. Catal. B: Environ.* 222 (2018) 176–181.
- [22] X.G. Duan, Z.M. Ao, D.G. Li, H.Q. Sun, L. Zhou, A. Suvorova, M. Saunders, G.X. Wang, S.B. Wang, *Carbon* 103 (2016) 404–411.
- [23] L.F. Lai, J.R. Potts, D. Zhan, L. Wang, C.K. Poh, C.H. Tang, H. Gong, Z.X. Shen, L.Y. Jianyi, R.S. Ruoff, *Energy Environ. Sci.* 5 (2012) 7936–7942.
- [24] S.N. Faisal, E. Haque, N. Noorbheesht, W.M. Zhang, A.T. Harris, T.L. Church, A.I. Minett, *RSC Adv.* 7 (2017) 17950–17958.
- [25] X.L. Li, H.L. Wang, J.T. Robinson, H. Sanchez, G. Diankov, H.J. Dai, *J. Am. Chem. Soc.* 131 (2009) 15939–15944.
- [26] N.I. Kotyukhova, P.J. Ollivier, B.R. Martin, T.E. Mallouk, S.A. Chizik, E.V. Buzaneva, A.D. Gorchinskiy, *Chem. Mater.* 11 (1999) 771–778.
- [27] H.Q. Sun, C. Kwan, A. Suvorova, H.M. Ang, M.O. Tade, S.B. Wang, *Appl. Catal. B: Environ.* 154 (2014) 134–141.
- [28] C. Galande, A.D. Mohite, A.V. Naumov, W. Gao, L.J. Ci, A. Ajayan, H. Gao, A. Srivastava, R.B. Weisman, P.M. Ajayan, *Sci. Rep.* 1 (2011).
- [29] M.P. Kumar, T. Kesavan, G. Kalita, P. Ragupathy, T.N. Narayanan, D.K. Pattanayak, *RSC Adv.* 4 (2014) 38689–38697.
- [30] X.X. Liu, D.L. Chao, Y. Li, J. Hao, X.S. Liu, J.P. Zhao, J.Y. Lin, H.J. Fan, Z.X. Shen, *Nano Energy* 17 (2015) 43–51.
- [31] A. Kumar, P.A. Lin, A. Xue, B.Y. Hao, Y.K. Yap, R.M. Sankaran, *Nat. Commun.* 4 (2013).
- [32] C. Zhang, X. Wang, Q.F. Liang, X.Z. Liu, Q.H. Weng, J.W. Liu, Y.J. Yang, Z.H. Dai, K.J. Ding, Y. Bando, J. Tang, D. Golberg, *Nano Lett.* 16 (2016) 2054–2060.
- [33] N.S. Xu, J. Chen, S.Z. Deng, *Diam. Relat. Mater.* 11 (2002) 249–256.
- [34] Q. Zou, Y.G. Li, L.H. Zou, M.Z. Wang, *Mater. Charact.* 60 (2009) 1257–1262.
- [35] H. Lee, H.J. Lee, J. Jeong, J. Lee, N.B. Park, C. Lee, *Chem. Eng. J.* 266 (2015) 28–33.
- [36] A. Dunlop, G. Jaskierowicz, P.M. Ossi, S. Della-Negra, *Phys. Rev. B* 76 (2007) 155403.
- [37] E. Perevedentseva, A. Karmenyan, P.H. Chung, Y.T. He, C.L. Cheng, *Surf. Sci.* 600 (2006) 3723–3728.
- [38] S. Indrawirawan, H.Q. Sun, X.G. Duan, S.B. Wang, *J. Mater. Chem. A* 3 (2015) 3432–3440.
- [39] G.H. Moon, Y. Park, W. Kim, W. Choi, *Carbon* 49 (2011) 3454–3462.
- [40] H. Elias, U. Götz, K.J. Wannowius, *Atmos. Environ.* 28 (1994) 439–448.
- [41] D.F. Evans, M.W. Upton, *J. Chem. Soc. Dalton Trans.* (1985) 1151–1153.
- [42] E.T. Yun, H.Y. Yoo, H. Bae, H.I. Kim, J. Lee, *Environ. Sci. Technol.* 51 (2017) 10090–10099.
- [43] Y.J. Yao, C. Lian, G.D. Wu, Y. Hu, F.Y. Wei, M.J. Yu, S.B. Wang, *Appl. Catal. B: Environ.* 219 (2017) 563–571.
- [44] E.A. Betterton, *Environ. Sci. Technol.* 26 (1992) 527–532.
- [45] G.P. Anipsitakis, D.D. Dionysiou, *Environ. Sci. Technol.* 38 (2004) 3705–3712.
- [46] X.G. Duan, H.Q. Sun, Y.X. Wang, J. Kang, S.B. Wang, *ACS Catal.* 5 (2015) 553–559.
- [47] P.M.D. Gara, G.N. Bosio, M.C. Gonzalez, N. Russo, M.D. Michelini, R.P. Diez, D.O. Martire, *Photochem. Photobiol. Sci.* 8 (2009) 992–997.
- [48] Y.P. Chin, G. Aiken, E. Oloughlin, *Environ. Sci. Technol.* 28 (1994) 1853–1858.
- [49] W.P. Johnson, G.B. Bao, W.W. John, *Environ. Sci. Technol.* 36 (2002) 608–616.
- [50] X.L. Wang, L. Shu, Y.Q. Wang, B.X. Xu, Y.C. Bai, S. Tao, B.S. Xing, *Environ. Sci. Technol.* 45 (2011) 9276–9283.
- [51] G.P. Anipsitakis, D.D. Dionysiou, M.A. Gonzalez, *Environ. Sci. Technol.* 40 (2006) 1000–1007.
- [52] Y. Yang, J.J. Pignatello, J. Ma, W.A. Mitch, *Environ. Sci. Technol.* 48 (2014) 2344–2351.
- [53] J.Y. Fang, C. Shang, *Environ. Sci. Technol.* 46 (2012) 8976–8983.
- [54] Z.S. Wei, F.A. Villamena, L.K. Weavers, *Environ. Sci. Technol.* 51 (2017) 3410–3417.
- [55] X. Chen, W.D. Oh, Z.T. Hu, Y.M. Sun, R.D. Webster, S.Z. Li, T.T. Lim, *Appl. Catal. B: Environ.* 225 (2018) 243–257.
- [56] S.L. Wang, N. Zhou, *Ultrason. Sonochem.* 29 (2016) 156–162.
- [57] P. Neta, V. Madhavan, H. Zemel, R.W. Fessenden, *J. Am. Chem. Soc.* 99 (1977) 163–164.
- [58] X.B. Wang, Y.L. Qin, L.H. Zhu, H.Q. Tang, *Environ. Sci. Technol.* 49 (2015) 6855–6864.
- [59] X.G. Duan, K. O'Donnell, H.Q. Sun, Y.X. Wang, S.B. Wang, *Small* 11 (2015) 3036–3044.